The Knowledge Engineering Review, Vol. 34, e22, 1 of 15.
doi:10.1017/S0269888919000171

Imitation of human motion for humanoid robot in lift and carry event

SHU-YIN CHIANG[1] and HAO-GE JIANG[2]

[1]*Department of Information and Telecommunications Engineering, Ming Chuan University, 5 De Ming Road, Gui Shan District, Taoyuan City 333, Taiwan;*
e-mail: sychiang@mail.mcu.edu.tw
[2]*School of Electrical and Electronic Engineering, Nanyang Technological University, 50 Nanyang Avenue, 639798, Singapore;*
e-mail: haoge001@ntu.edu.sg

Abstract

This study proposed a method to enable a humanoid robot to step up onto a stair by imitating the step-up motion of a human and to accomplish a lift and carry event in HuroCup of Federation of International RoboSports Association. The step-up motion, divided into five states, was captured by a Kinect sensor, and the human joints corresponded to the humanoid robot joints. Selected servomotors and their angle variation were matched with that of human joint numbers by a designed fuzzy inference system on the basis between the human and the humanoid robot joints. Then, the rest of the robot motors were adjusted by the zero moment point obtained from force-sensing registers to maintain stability. Next, two intermediate transition states were added between each state of the humanoid robot step-up to maintain its balance and reduce motor damage. Finally, to be applied in a real lift and carry event, a vision system was integrated to recognize the edge of a color board and determine a suitable site for the step-up. With these functions integrated, the robot under the proposed method was verified to successfully achieve the task of the lift and carry event without losing its balance or falling.

1 Introduction

Humanoid robots are human-like figures that are primarily expected to make various human-like motions. The completion idea of the Federation of International RoboSports Association (FIRA) is to make robots that can perform all kinds of sports activities as humans do. For example, the FIRA HuroCup is held with several events that are similar but simpler versions of human sports events. For the humanoid robot stair-climbing task, previous research (Gutmann *et al.*, 2004; Fu and Chen 2008) has discussed the force and kinematics of the humanoid robot. Much research has focused on how to modify the programming codes or develop an algorithm for the robot to complete the tasks. The goal of this work is to successfully complete the task of lift and carry in the FIRA HuroCup competition by imitating human motion.

The imitation of human motion by humanoid robots was proposed by Calderon and Hu (2005) and Nakazawa *et al.* (2002). Koenemann *et al.* (2014) suggested a system in which humanoid robots can imitate human body movements in real time by taking into account the end positions of the feet, arms, and the center of mass. Poubel *et al.* (2014) proposed imitating human motion through instant simulation. Both imitation systems are based on inverse kinematics (Williams, 2012) to obtain the related motor angles for the robot (Nguyen and Lee 2012). However, balance control remains an issue.

For the imitation of human motion, the Kinect sensor is the most popular device to capture the human skeleton (Field *et al.*, 2011; El-Iaithy *et al.*, 2012). However, the difficulty lies in mapping the joints obtained from the Kinect sensor to those of a humanoid robot because of the degree of freedom (DOF) difference and whether the balance control system is supported by muscles.

Table 1 DWRwIn-OP servomotor ID position and angle.

Robot ID	Robot position	Angle	Robot ID	Robot position	Angle
1	R_Shoulder_Pitch	θ_1	11	R_Hip_Pitch	θ_{11}
2	L_Shoulder_Pitch	θ_2	12	L_Hip_Pitch	θ_{12}
3	R_Shoulder_Roll	θ_3	13	R_Knee	θ_{13}
4	L_Shoulder_Roll	θ_4	14	L_Knee	θ_{14}
5	R_Elbow	θ_5	15	R_Ankle_Pitch	θ_{15}
6	L_Elbow	θ_6	16	L_Ankle_Pitch	θ_{16}
7	R_Hip_Yaw	θ_7	17	R_Ankle_Roll	θ_{17}
8	L_Hip_Yaw	θ_8	18	L_Ankle_Roll	θ_{18}
9	R_Hip_Roll	θ_9	19	Head_Pan	θ_{19}
10	L_Hip_Roll	θ_{10}	20	Head_Tilt	θ_{20}

Figure 1 Schematic of the DARwIn-OP servomotor numerically assigned positions

Considering this difficulty, this work proposes an algorithm with a Kinect sensor and achieves the goal of a humanoid robot performing the task of lift and carry in HuroCup competition by imitating the motion of a human to maintain its balance. The rest of the paper is structured as follows. Section 2 describes the problem of obstacles and introduces the humanoid robot used in this study. A fuzzy logic algorithm is proposed in Section 3. The experimental results are presented in Section 4, and the paper concludes in Section 5.

2 Humanoid robot and the problem description

2.1 Humanoid robot

Figure 1 shows the 45.5-cm-tall humanoid robot DARwIn-OP, which is an abbreviation for Dynamic Anthropomorphic Robot with Intelligence-Open Platform. DARwIn-OP, developed by ROBOTIS, operates with a 1.6 GHz Intel Atom Z530 (32-bit) onboard 4 GB flash solid-state drive and comprises 20 Dynamixel MX-28 actuators. The actuators offer 6-DOF leg movement, dual 3-DOF arm movement, and dual 2-DOF neck movement. The robot is equipped with a Universal Serial Bus (USB 2.0) high-definition Logitech C905 camera and has a three-axis gyroscope and a three-axis accelerometer as sensors to complete the task in the HuroCup competition. The motor ID and the related angles are defined in Table 1,

Figure 2 Photograph of the robot performing the lift and carry event

where R indicates the right side and L represents the left side. Four force-sensing register (FSR) modules (Ha *et al*., 2013) are placed in each foot for ground reaction force measurements. These FSRs are used to find the zero moment point (ZMP), which indicates the most stable region of the robot.

2.2 Problem description

For the HuroCup competition, the robot needs to step up to irregularly shaped differently colored boards according to the rules of FIRA's lift and carry event. The challenge in this event is that the height of the board for each step is approximately 1.8–2.0 cm, as shown in Figure 2. To perform the step-up motion successfully, the robot must automatically recognize the edge of the color boards.

3 Proposed algorithm

For the humanoid robot to step up onto the boards autonomously, we proposed the following algorithm:

Step 1. Use the imitation system to find the related core motor angles from the human to the humanoid robot by the fuzzy logic system described in Sections 3.1 and 3.2.
Step 2. Initialize the rest of the motors and adjust their parameters according to the ZMP stable region of feet from the FSR of both feet, as explained in Section 3.3.
Step 3. Increase the intermediate states between the stable states and the transition states (see Section 3.3).

3.1 Human motion imitation

To accomplish the lift and carry task, the robot is designed based on imitations of human motion. Human motion is captured by a Kinect v2 sensor, and the corresponding skeletal joints are recorded and screened by a personal computer, as shown in Figure 3. To make the original and imitated motion consistently, the number of human joints, captured by the Kinect as shown in Figure 3(a) and (b), is modified according to the servomotor ID of DARwIn-OP.

Next, the Kinect records the human motion of stepping up in three different views so that the motion can be analyzed and applied to train the robot. These three views of human motion—side, front, and top—are shown in Figures 4–6, respectively. The joints of human motion are not easily recognized; hence, the different views provide more recognizable motion for further analysis. The motion of stepping up is divided into five states, and the depth images for each state from the Kinect are shown in Figure 4. In Figure 4(a), the human is standing up in a ready position. The human now raises its left foot to step up to a stair (Figure 4(b)). Then, the human adjusts its center of mass by lowering its body and maintains balance by moving its arms, as shown in Figure 4(c). Next, the human keeps its left foot on the stair and raises its right foot to the stair, as seen in Figure 4(d). Finally, the human finishes the step-up task (Figure 4(e)).

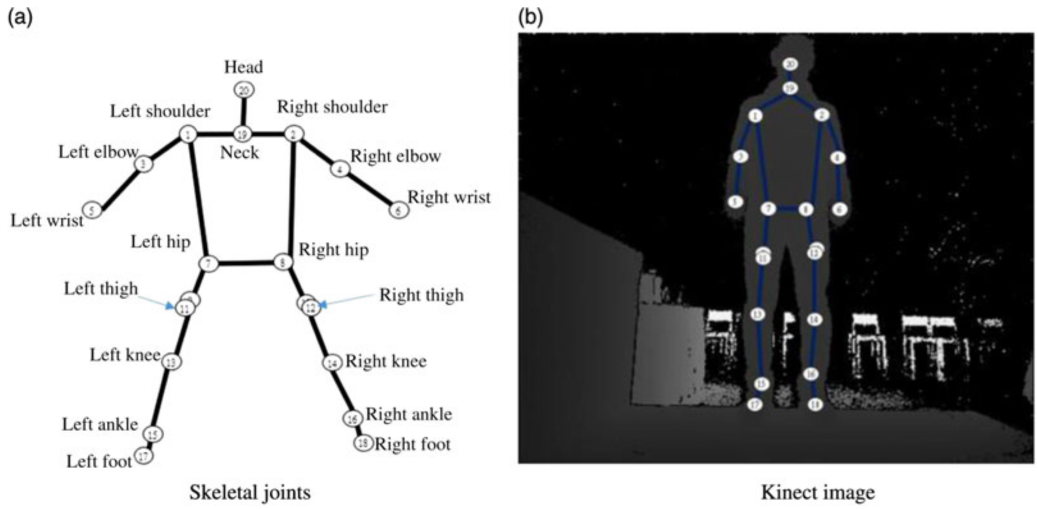

Figure 3 Twenty human skeletal joints captured by the Kinect. (a) Skeletal joints. (b) Kinect image

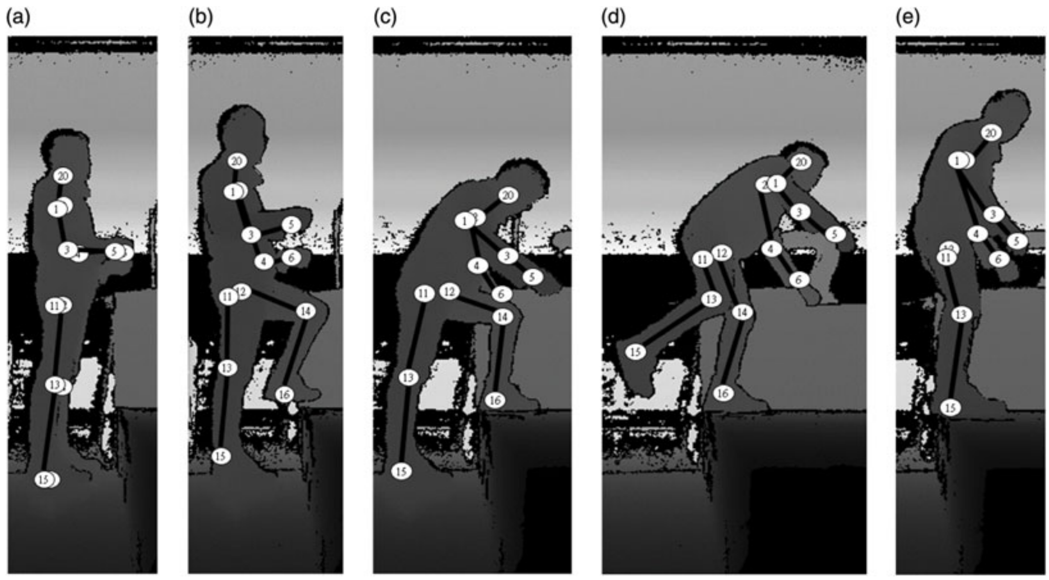

Figure 4 Five states of the human step-up motion from the side view

3.2 Data analysis and fuzzy algorithm

Simple geometrical operations are used to calculate the angles between vectors, as shown in Equations (1) and (2), where $\mathbf{V}_{\mathrm{C3C1}}$ represents the vector of the left elbow to the left and $\mathbf{V}_{\mathrm{C3C5}}$ represents the vector of left elbow to left wrist as shown in Figure 7, and then the joint angle for left elbow can be calculated by vectors $\mathbf{V}_{\mathrm{C3C1}}$ and $\mathbf{V}_{\mathrm{C3C5}}$

$$\overrightarrow{\mathbf{V}_{C_3C_1}} \times \overrightarrow{\mathbf{V}_{C_3C_5}} = \left|\overrightarrow{\mathbf{V}_{C_3C_1}}\right| \left|\overrightarrow{\mathbf{V}_{C_3C_5}}\right| \cos(\theta_{LE}) \quad (1)$$

$$\theta_{LE} = \cos^{-1}\left(\frac{\overrightarrow{\mathbf{V}_{C_3C_1}} \times \overrightarrow{\mathbf{V}_{C_3C_5}}}{\left|\overrightarrow{\mathbf{V}_{C_3C_1}}\right| \left|\overrightarrow{\mathbf{V}_{C_3C_5}}\right|}\right) \quad (2)$$

However, there are several differences between a human body and a humanoid robot. For example, the difference in the DOF between humans and humanoid robots was discussed by Zheng *et al*. (2012). Hence, direct movement mapping between a human arm and a humanoid robot arm is not feasible owing to differences in kinematics and dynamics parameters. Instead, the humanoid robot has to imitate human

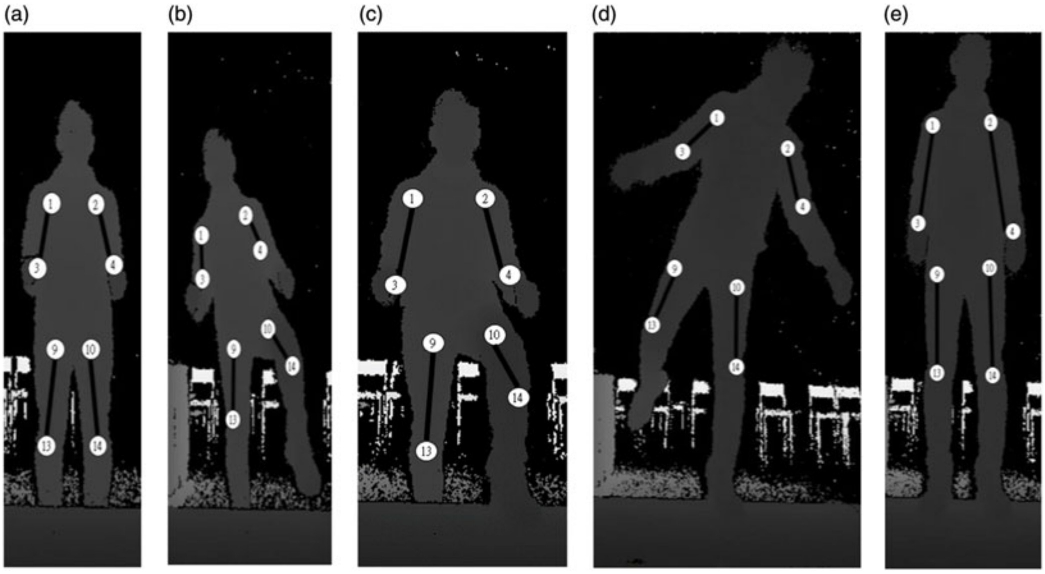

Figure 5 Five states of the human step-up motion from the front view

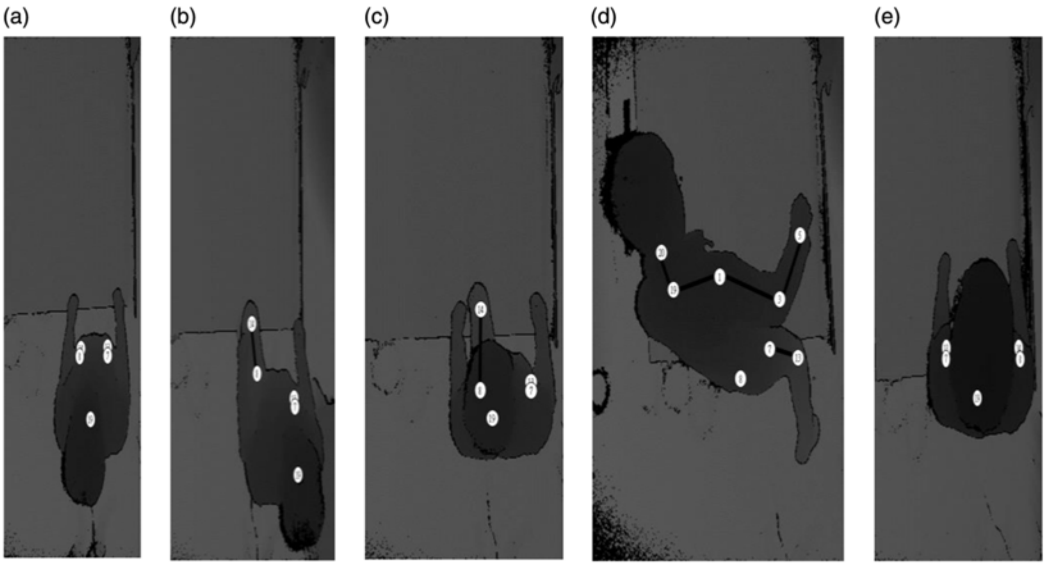

Figure 6 Five states of the human step-up motion from the top view

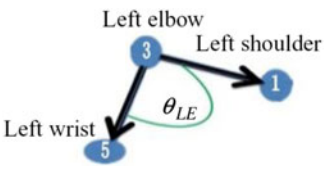

Figure 7 Schematic showing the angle calculation

motion. The angles of the human step-up motion for five stages are listed in Table 2. The ID number is the same as that listed in Table 2. Because R_Hip_Yaw (ID 7), L_Hip_Yaw (ID 8), R_Ankle_Roll (ID 17), and L_Ankle_Roll (ID 18) are not available from the depth image, and the head (ID 19 and ID 20) does not move during the step-up process, servomotor IDs 7, 8, 17, 18, 19, and 20 are excluded in Table 2. In Table 2, IDs 1, 2, 11, and 12 are marked in blue. Because IDs 1 and 2 control robot arm movement and IDs 11 and 12 control robot body tilt, these four IDs significantly vary during the step-up process.

Table 2 Angles of human step-up motion for the five stages.

ID	Stage 1	Stage 2	Stage 3	Stage 4	Stage 5
1	29	31	80	75	70
2	29	31	65	95	65
3	−25	−15	−35	−5	−30
4	25	15	23	57	26
5	65	60	45	55	65
6	66	105	75	45	65
9	15	14	16	21	15
10	15	10	17	21	20
11	0	−15	15	67	15
12	0	36	89	63	26
13	0	0	−67	−30	−15
14	0	−75	−85	−70	−60
15	85	85	105	75	90
16	85	115	105	100	90

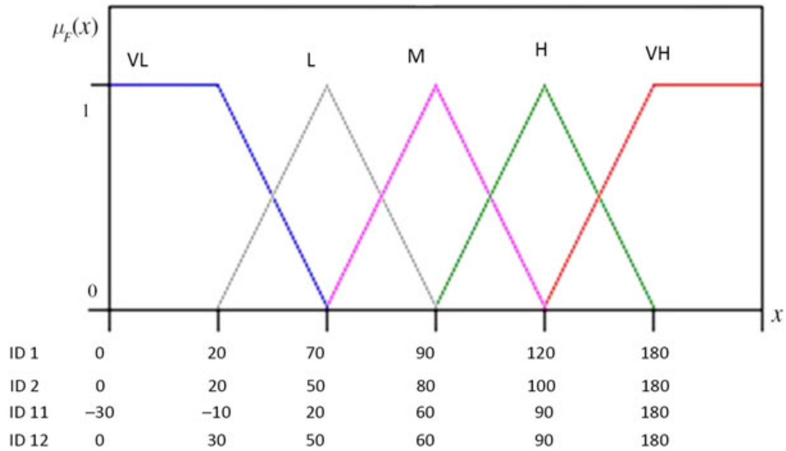

Figure 8 Membership functions for each input X_i

The remaining IDs have less variation during the step-up process. These four motors were selected to be involved in the designed fuzzy logic rule because they control the balance of the robot and thus are the most significant factors influencing its step-up motion.

The fuzzy logic system is designed as follows (Betin *et al.*, 2000; Zhao and Bose, 2002). The parameter degree obtained from the human is called ϕ_i, and $i = 1, 2, 11$, and 12 are the inputs called X_i in the fuzzy system. Each parameter X_i will be fuzzed into value within the range [0, 1], and the membership functions are very low (VL), low (L), medium (M), high (H), and very high (VH). The membership functions evaluate the ability x belonging to the set F denoted by $\mu_F(x)$, in which x is the value of the estimated parameter and F is a set of real values within the range [0, 1], as defined in Figure 8. Even though different motors have different values for VL, L, M, H, and VH, these values are used to classify the fuzzy range of inputs. Fuzzy sets: $F \in \{\text{VL, L, M, H, VH}\}$, μF is the degree of the membership function for input fuzzy set F, {0 20 70 90 120 180}, {0 20 50 80 100 180}, {−30 −10 20 60 90 180}, and {0 30 50 60 90 180} are the values of input fuzzy set F for IDs 1, 2, 11, and 12, respectively.

Next, the single-input and single-output fuzzy inference systems are adapted to define the fuzzy rule if. . . then. . . as follows:

Rule 1:	If X_i is very low,	then Y_i is very low.
Rule 2:	If X_i is low,	then Y_i is low.
Rule 3:	If X_i is medium,	then Y_i is medium.
Rule 4:	If X_i is high,	then Y_i is high.
Rule 5:	If X_i is very high,	then Y_i is very high.

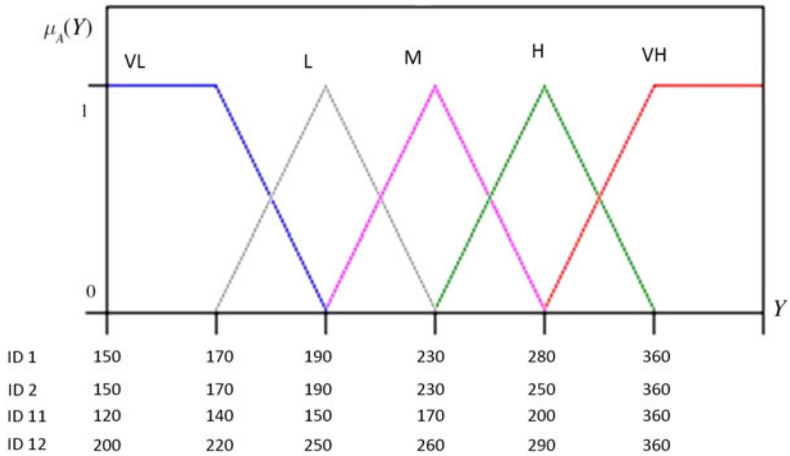

Figure 9 Membership functions for each output Y_i

Similarly, membership function evaluates the ability Y_i belonging to the set A denoted $\mu_A(y)$, in which y is the value of an estimated parameter and A is a set of real values within the range [0, 1] as defined in Figure 9. Finally, based on the fuzzy methodology, the center of gravity method is applied in this study to obtain the related output Y_i which is the angle of motor ID 1, ID 2, ID 11, and ID 12 for the robot as shown in Equation (3).

$$Y_i^* = \frac{\int_{y_i \in Y} \mu_A(y_i) \cdot y_i \, dy_i}{\int_{y_i \in Y} \mu_A(y_i) \, dy_i} \tag{3}$$

After the fuzzy algorithm calculation, the relationship between the angle variation in the human and robot step-up motion for IDs 1, 2, 11, and 12 is plotted (Figure 10).

3.3 Robot motion adjustment and balance

Inside the sole area of the support foot, the FSR maps the current pressure point at which the whole body exerts its weight. The position values acquired from the FSR mounted in the DARwIn-OP humanoid are represented with integral quantities ranging from 0 to 254, as shown in Figure 11. For the double-stand phase of the humanoid robot, the stable region of the ZMP (the red rectangular region in Figure 11) is tested (Chien *et al.*, 2015) and is located at the center of both feet.

The related motors are adjusted to find a stable position for the humanoid robot (Figure 12). First, the related parameters of the robot are imported to the algorithm to obtain the ZMP from the FSRs of both feet. Next, a decision-making process is followed to adjust the related parameters of the motors to ensure that the ZMP from the FSR is in the stable region. If the ZMP is too far to the left, motor IDs 4, 6, 10, and 14 on the left side of the robot are adjusted. Similarly, if the ZMP is too far to the right, motor IDs 3, 5, 9, and 13 on the right side of the robot are adjusted. If the ZMP of the robot is too forward, related motor IDs 1, 2, 11 and 12 are adjusted to make the robot move its center of mass to the back and vice versa.

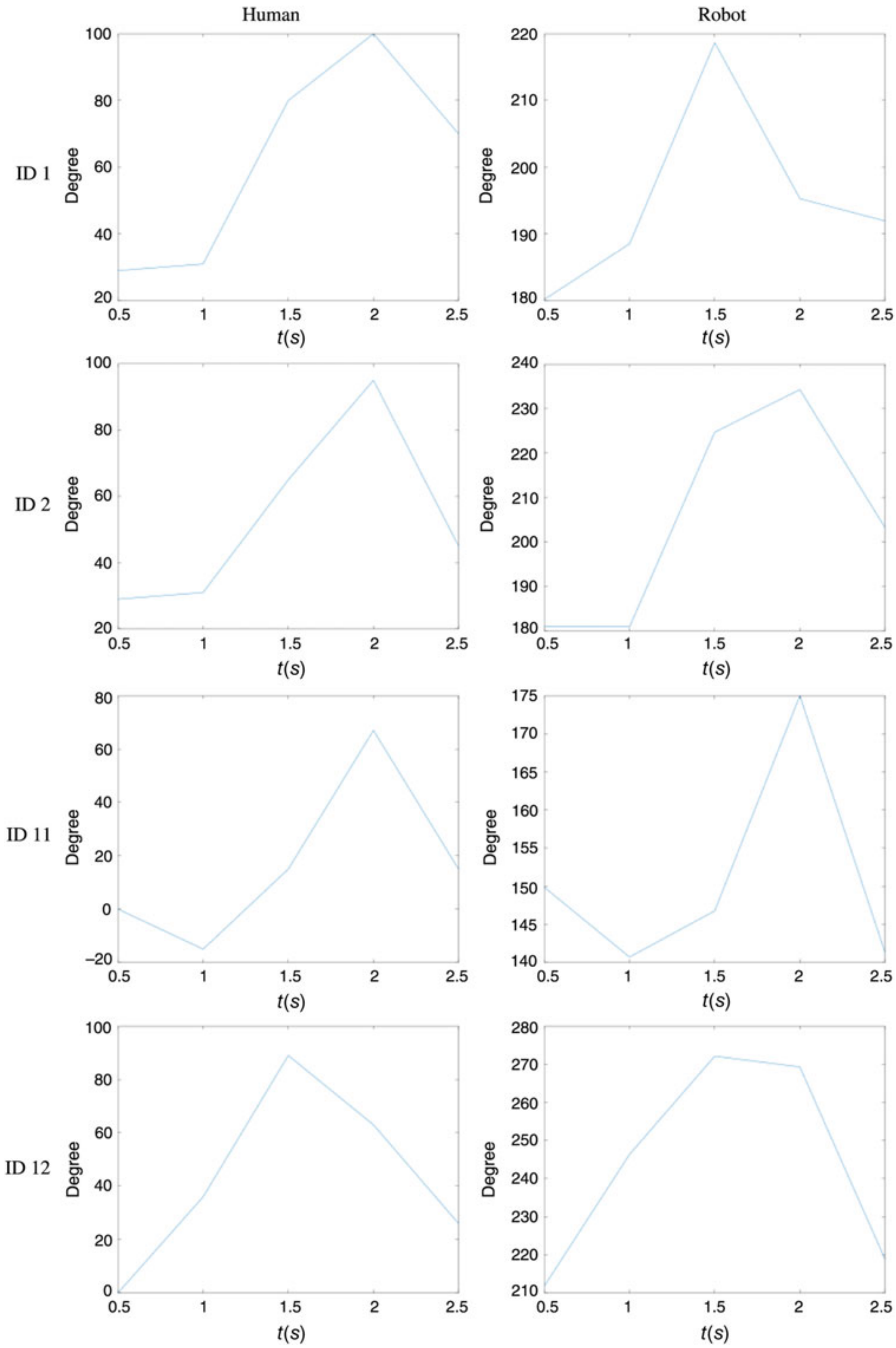

Figure 10 Designed ID angle variation for the human and robot step-up motion

The ZMP is determined by the values of FSR. Then, the ZMP is adjusted based on the rule described below. If ZMP is too left, the motor IDs 4, 6, 10, and 14 are modified with a value $\Delta\theta_i$, $i = 4, 6, 10$ and 14 as shown in Table 3. The listed values were obtained by experiments. The method is also applied when ZMP is at right, forward, and backward, respectively. If the motor needs to rotate clockwise, the angle increases with a small amount; otherwise, the angle decreases. The adjustment for ZMP is summarized in Table 3.

Table 3 ZMP adjustment for Figure 12

Left	Right	Forward	Backward
$\theta_4 = \theta_4 - \Delta\theta_4$	$\theta_3 = \theta_3 + \Delta\theta_3$	$\theta_1 = \theta_1 + \Delta\theta_1$	$\theta_1 = \theta_1 - \Delta\theta_1$
$\theta_6 = \theta_6 + \Delta\theta_6$	$\theta_5 = \theta_5 - \Delta\theta_5$	$\theta_2 = \theta_2 - \Delta\theta_2$	$\theta_2 = \theta_2 + \Delta\theta_2$
$\theta_{10} = \theta_{10} + \Delta\theta_{10}$	$\theta_9 = \theta_9 - \Delta\theta_9$	$\theta_{11} = \theta_{11} + \Delta\theta_{11}$	$\theta_{11} = \theta_{11} - \Delta\theta_{11}$
$\theta_{14} = \theta_{14} - \Delta\theta_{14}$	$\theta_{13} = \theta_{13} + \Delta\theta_{13}$	$\theta_{12} = \theta_{12} - \Delta\theta_{12}$	$\theta_{12} = \theta_{12} + \Delta\theta_{12}$

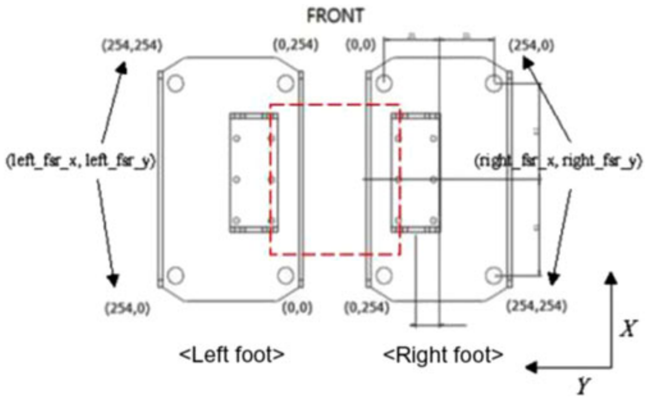

Figure 11 Definition of FSR values and the stable region for the DARwIn-OP humanoid

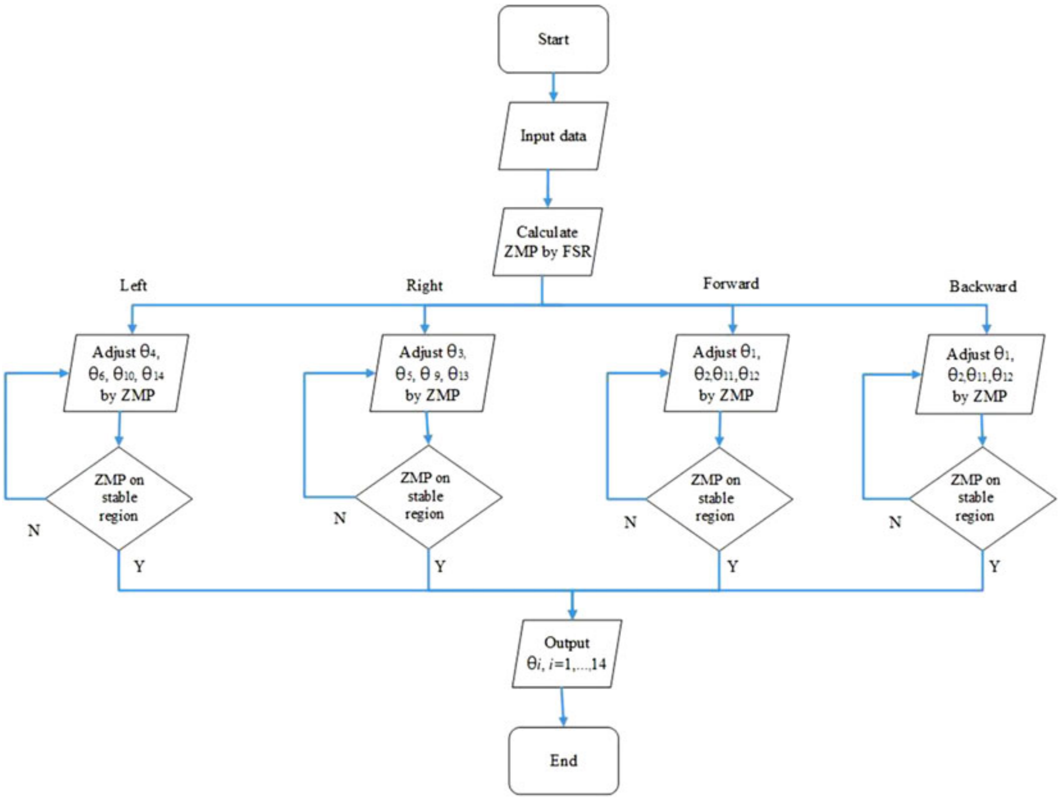

Figure 12 Flowchart showing how to adjust the robot position to be stable according to the ZMP

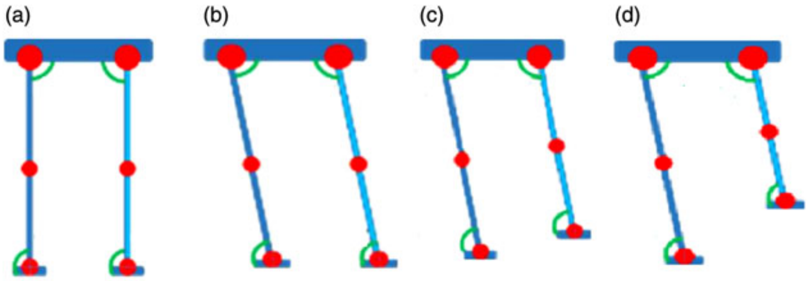

Figure 13 Adding transition steps in the robot's motion to maintain balance

Moreover, motor IDs 15, 16, 17, and 18 may affect the balance of the robot as well. The motors IDs 15 and 16 control the soles of the feet to left or right, while IDs 17 and 18 control them forward or backward. Therefore, the angles of those motors are within −15° to 15° to keep the soles of the feet parallel to the ground in X and Y planes so that the robot can step on the stairs with its entire feet and prevent itself from tripping.

Besides, a humanoid robot cannot move from one step to another step directly because suddenly changing position leads to balance loss and falling. Therefore, for a humanoid robot, a transition state (Chiang *et al.*, 2017), as illustrated in Figure 13, is required for balance and motor protection. The robot is designed so that it moves from a standing straight position (Figure 13(a)) to raise the right foot up (Figure 13(d)). In the process, two more steps, shown in Figure 13(b) and (c), are added to the transition state to maintain balance. These steps are added in the step-up motion of the robot for each of the five stages.

To handle a wide range of transitions, we also consider the case where two points (such as in Figure 13(a) and (d)) in the state space cannot be joined in one step. Specifically, given two states, S_i and S_j, we design transition states or two intermediate states – ${S_a}^{i\to j}$ (Figure 13(b)) and ${S_b}^{i\to i}$ (Figure 13(c)) (Da *et al.*, 2017), as shown in Equation (4) – and the corresponding control parameters so that the robot transitions are implemented. The transition state is obtained by linear interpolation, as shown in Equations (5) and (6).

$$S_i \to S_a^{i\to j} \to S_b^{i\to j} \to S_j \tag{4}$$

$$S_a^{i\to j} = \alpha\, S_i(\Theta) + (1-\alpha)\ S_j(\Theta) \tag{5}$$

$$S_b^{i\to j} = \beta\, S_i(\Theta) + (1-\beta)\ S_j(\Theta) \tag{6}$$

where $\alpha \in (0, 1)$, $\beta \in (0, 1)$, and Θ are all motors parameters.

3.4 Robot vision system

The robot is supposed to autonomously walk to and step up onto each color board in the lift and carry event. Thus, the vision system is used to recognize the color of the board and find a suitable step-up position. This position is the site where the robot's balance is most likely to be maintained, with the size of the robot feet (10.4 cm in depth and 16.5 cm in width) taken into consideration. Thus, the relationship between the pixel size in the image and the real size of the color board, as shown in Figure 14 from the view of the robot, must be obtained. Next, the depth vector **D**, defined in Equation (7), is a 1 × 32 dimension vector and is obtained from the first color board location from the bottom row for each column, as shown in Figure 15(a).

$$\mathbf{D} = [d_1, d_2, \cdots, d_{32}] \tag{7}$$

$$\text{If } d_i < T,\ \text{ for } i = 1, \ldots, 32, \text{ then step up} \tag{8}$$

Here, d_i is the distance from the first color board grid location to the robot for the ith column.

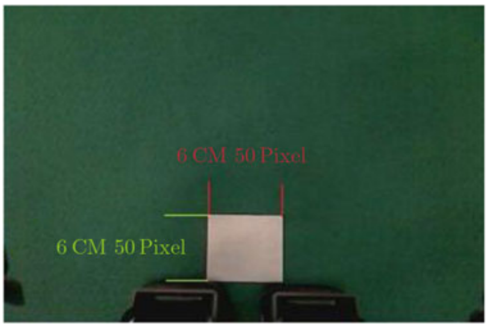

Figure 14 The relationship between pixels versus dimension

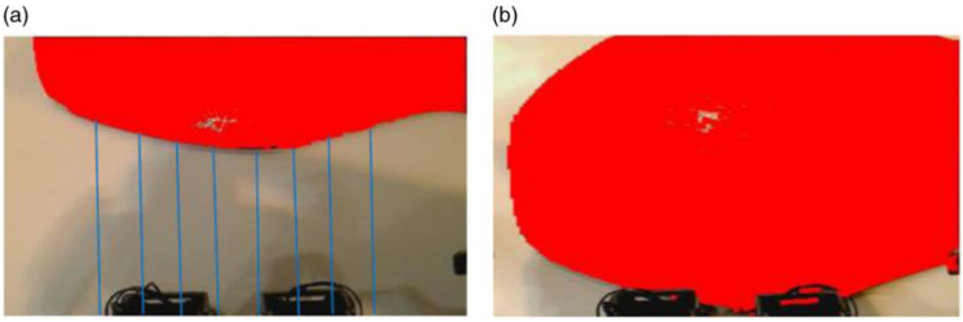

Figure 15 The robot tries to find the edge of the color board

Then, every d_i is calculated. If all the di are less than the threshold value T (in this experiment, $T = 7$ pixels) as described in Equation (8), then the robot has hit the edge of the color board, as shown in Figure 15(b).

4 Performance analysis

In Section 3, the imitation process of the robot to finish the lift and carry task is analyzed. To demonstrate the results of the proposed algorithm, we show the one step of lift and carry in Figure 16. In Figure 16(a)–(c), state S_1 to state S_2 is carried out with two additional transition states or intermediate states ${S_a}^{1\to2}$ and ${S_b}^{1\to2}$, as described in Section 3.3, to keep the robot in balance. Transition or intermediate states are also applied for states S_2 to S_4, as shown in Figure 16(d)–(l). Finally, the robot finishes the fifth state of stepping up a stair (Figure 16(m)).

The FSR of the robot during the proposed algorithm from imitation of human motion is plotted in Figure 17. In Figure 17(a) state 1, the robot is in the double-stand phase; hence, the ZMP marked in blue is the sum of both FSRs marked in red. In Figure 17(b) and (c), state ${S_a}^{1\to2}$ and state ${S_b}^{1\to2}$ are single-stand phases; the robot stands on its right foot only, and the left FSR is not shown in Figure 17(b) and (c). Therefore, the ZMP is only the right FSR for both states. In Figure 17(d)–(h), the robot is back to the double-stand phase; hence, the ZMP is the sum of both FSRs. In Figure 17(i)–(k), the robot is in a single-stand phase and stands on its left foot; hence, the FSR of the right foot is missing. Finally, the robot returns to the double-stand phase, with the ZMP shown at the center of both feet in Figure 17(l) and (m). To view the transition of the ZMP, the FSR from state 1 to state 5 is marked as 1–13. The right FSR is marked in green as Ri, $i = 1, \ldots, 13$, and the left FSR is marked in red as Li, $i = 1, \ldots, 13$. The sum of both FSRs is marked in blue as Mi, $i = 1, \ldots, 13$ (Chien *et al.*, 2015). The result is shown in Figure 18. In Figure 18, all the states with the double-stand phase are in a stable region. Even though the single states are not in the ZMP stable region, in the next double-stand phase, the robot is in the stable region. Hence, the robot can imitate human motion to finish the life and carry event, while maintaining stable positions.

To illustrate the performance and availability of the proposed algorithm in a real contest, an experimental environment is set up based on the rules of the lift and carry event (Figure 19).

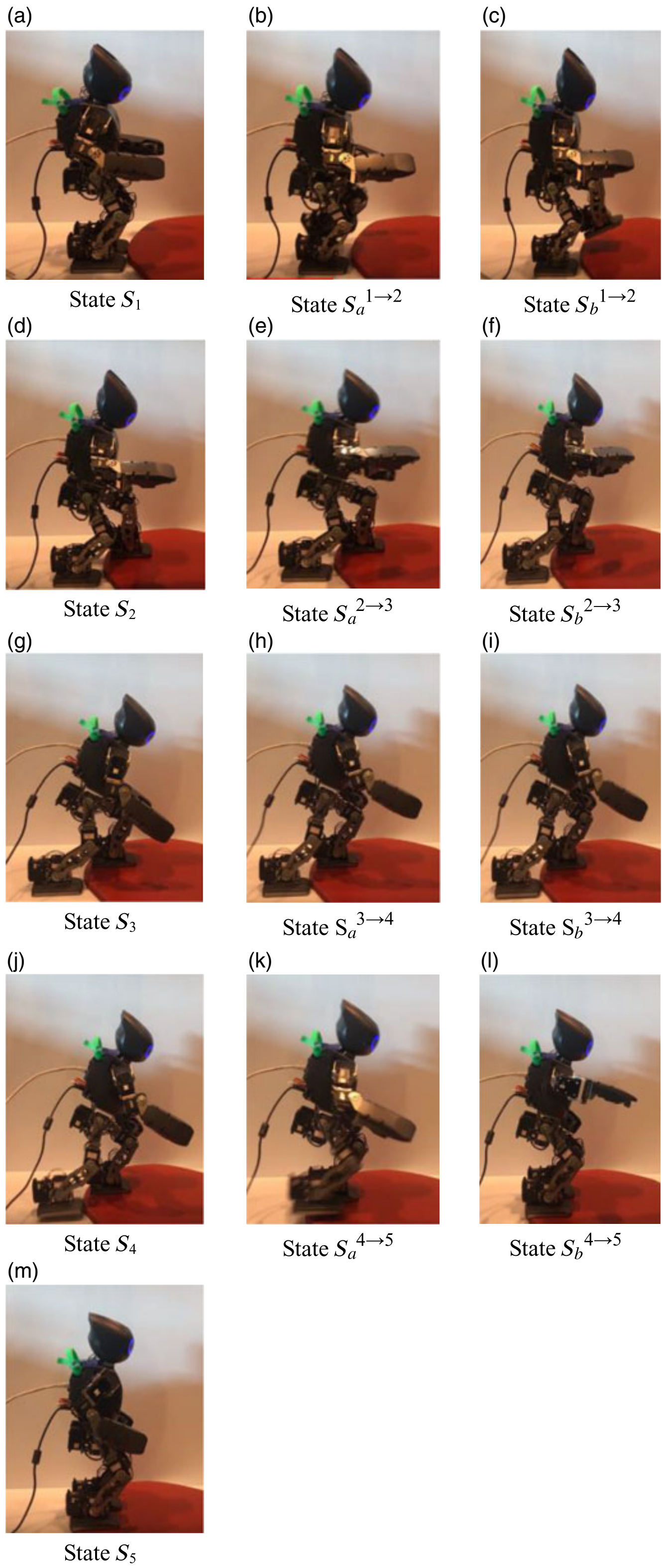

Figure 16 Experimental result of the proposed algorithm from imitation of human motion. (a) State S_1. (b) State $S_a^{1\to2}$. (c) State $S_b^{1\to2}$. (d) State S_2. (e) State $S_a^{2\to3}$. (f) State $S_b^{2\to3}$. (g) State S_3. (h) State $S_a^{3\to4}$. (i) State $S_b^{3\to4}$. (j) State S_4. (k) State $S_a^{4\to5}$. (l) State $S_b^{4\to5}$. (m) State S_5

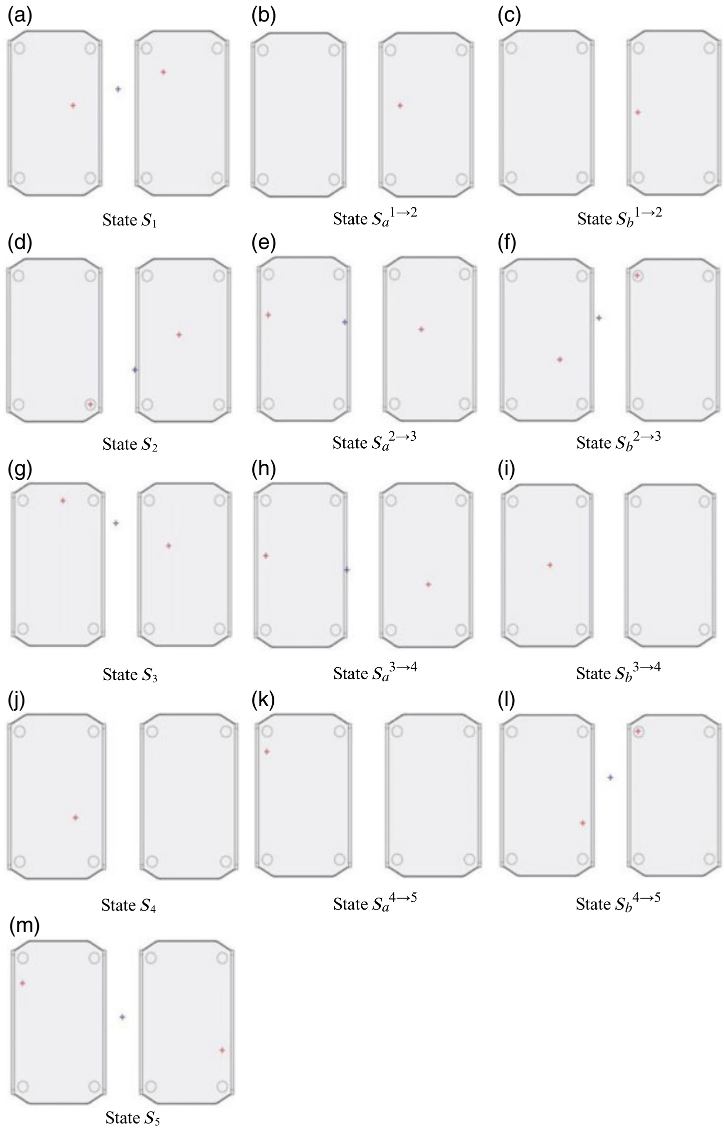

Figure 17 FSR results of the proposed algorithm from imitation. (a) State S_1. (b) State $S_a{}^{1\to2}$. (c) State $S_b{}^{1\to2}$. (d) State S_2. (e) State $S_a{}^{2\to3}$. (f) State $S_b{}^{2\to3}$. (g) State S_3. (h) State $S_a{}^{3\to4}$. (i) State $S_b{}^{3\to4}$. (j) State S_4. (k) State $S_a{}^{4\to5}$. (l) State $S_b{}^{4\to5}$. (m) State S_5

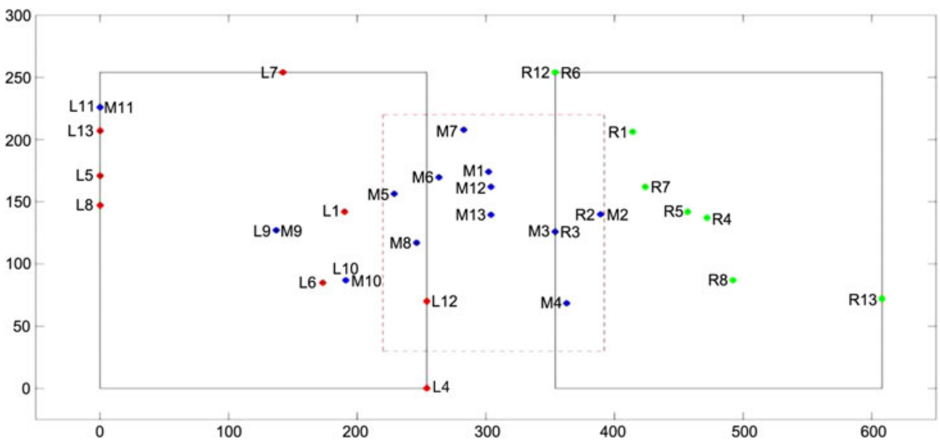

Figure 18 FSR and ZMP for all states

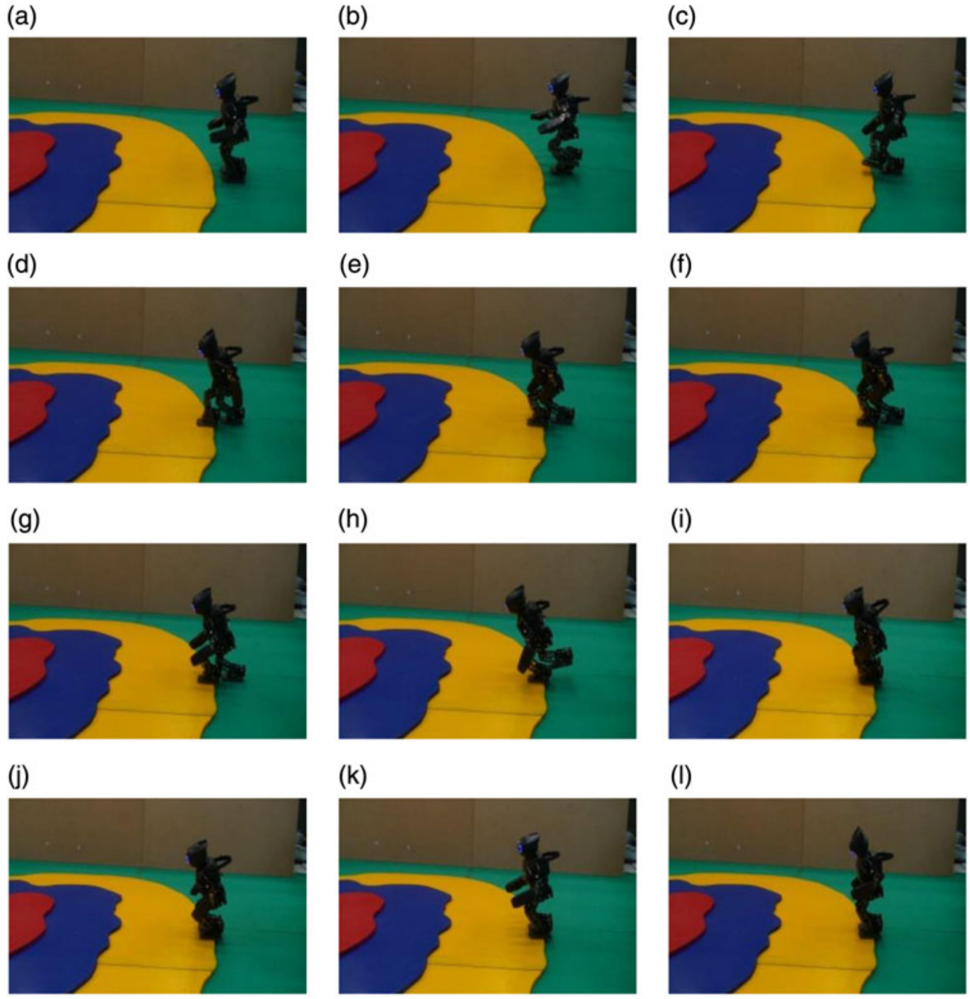

Figure 19 Experimental result of the proposed algorithm with the vision system

5 Conclusions

This study proposed a method to enable a humanoid robot, DARwIn-OP, to imitate the step-up motion of a human and accomplish a lift and carry event in the HuroCup competition. First, human motion was captured by a Kinect sensor, and the positions of human joints and humanoid robot joints were made to correspond. Next, the human step-up motion was divided into five stages and analyzed separately. Then, servomotor IDs 1, 2, 11, and 12 were selected, and their angle variation was matched with that of human joint numbers 1, 2, 11, and 12 by designed fuzzy logic rules based on the difference in the DOF between the joints of a human and a humanoid robot. In addition, a process for maintaining a stable position was discussed by means of the ZMP region to adjust the parameters of the related motor according to ZMP. Two additional transition states were incorporated for each stage of the humanoid robot step-up motion to maintain its balance and reduce motor damage. Finally, for application in a real lift and carry event, the vision system was integrated to recognize the edge of the color board and determine a suitable site for the step-up. With these functions integrated, the robot under the proposed method was verified to successfully complete the lift and carry event without losing its balance or falling. As a result, this method can be applied to different types of humanoid robots.

References

Betin, F., Pinchon, D. & Capolino, G.-A. 2000. Fuzzy logic applied to speed control of a stepping motor drive. *IEEE Transactions on Industrial Electronics* **47**, 610–622, Jun 2000.

Calderon, C. A. & Hu, H. 2005. Robot imitation from human body movements. In *Proceedings of the third International Symposium on Imitation in Animals and Artifacts*, 1–9.

Chiang, S.-Y., Kuo, S.-C., Lin, J.-B. & Chen, C.-H. 2017. Dynamic imitation of human motion for humanoid robot. In *IEEE Smart World Congress*, DOI: 10.1109/UIC-ATC.2017.8397437.

Chien, D. V., Sung, K. J. & Kim, J.-W. 2015. Sensory reflex control of a humanoid robot using FSR sensor. In *IEEE International Conference on Advanced Intelligent Mechatronics (AIM)*, 1406–1409.

Da, X., Hartley, R. & Grizzle, J. W. 2017. Supervised learning for stabilizing underactuated bipedal robot locomotion, with outdoor experiments on the wave field. In *IEEE International Conference on Robotics and Automation (ICRA)*, 3476–3483.

El-Iaithy, R. A., Huang, J. & Yeh, M. 2012. Study on the use of Microsoft Kinect for robotics applications. In *IEEE Position Location and Navigation Symposium*, 1280–1288.

Field, M., Pan, Z., Stirling, D. & Naghdy, F. 2011. Human motion capture sensors and analysis in robotics. *Industrial Robot: An International Journal* **38**, 163–171.

Fu, C. & Chen, K. 2008. Gait synthesis and sensory control of stair climbing for a humanoid robot. *IEEE Transactions on Industrial Electronics* **55**, 2111–2120.

Gutmann, J.-S., Fukuchi, M. & Fujita, M. 2004. Stair climbing for humanoid robots using stereo vision. In *Proceedings 2004 international Conference on Intelligent Robots and Systems*, 1407–1413.

Ha, I., Tamura, Y. & Asama, H. 2013. Development of open platform humanoid robot DARwIn-OP. In *SICE Annual Conference*, 2178–2181.

Koenemann, J., Burget, F. & Bennewitz, M. 2014. Real-time imitation of human whole-body motions by humanoids. In *2014 IEEE International Conference on Robotics & Automation (ICRA)*, 2806–2812.

Nakazawa, A., Nakaoka, S., Ikeuchi, K. & Yokoi, K. 2002. Imitating human dance motions through motion structure analysis. *Proceedings of IEEE/RSJ International Conference on Intelligent Robots and Systems* **3**, 2539–2544.

Nguyen, V. V. & Lee, J.-H. 2012. Full-body imitation of human motions with Kinect and heterogeneous kinematic structure of humanoid robot. In *Proceedings of IEEE/SICE International Symposium on System Integration*, 93–98.

Poubel, L. P., Sakka, S., Ćehajić, D. & Creusot, D. 2014. Support changes during online human motion imitation by a humanoid robot using task specification. In *IEEE International Conference on Robotics & Automation (ICRA)*, 1782–1787.

Williams, R. L. II. 2012. DARwIn-OP humanoid robot kinematics. *ASME 2012 International Design Engineering Technical Conferences and Computers and Information in Engineering Conference*, **4**, 1187–1196.

Zhao, J. & Bose, B. K. 2002. Evaluation of membership functions for fuzzy logic controlled induction motor drive. In *IEEE Annual Conference of Industrial Electronics Society*, 229–234.

Zheng, X., Fu, M., Yang Y. & Lv, N. 2012. 3D human postures recognition using Kinect. In *Proceedings of the 4th International Conference on Intelligent Human-Machine Systems and Cybernetics*, 344–347.